Tunable 2D-gallium arsenide and graphene bandgaps in a graphene/GaAs heterostructure : an ab initio study

Journal of Physics: Condensed Matter

ACCEPTED MANUSCRIPT

# Tunable 2D-gallium arsenide and graphene bandgaps in graphene/GaAs heterostructure: An ab-initio study

To cite this article before publication: Alvaro González-García *et al* 2019 *J. Phys.: Condens. Matter* in press https://doi.org/10.1088/1361-648X/ab0d70

# Tunable 2D-Gallium Arsenide and Graphene bandgaps in Graphene/GaAs heterostructure: An *ab-initio* study

**A. González-García [1 2], W. López-Pérez[1], R. González-Hernández[1], J. A. Rodríguez[3], M. V. Milosevic[2], and F. M. Peeters[2]**

[1] Grupo de Investigación en Física Aplicada, Departamento de Física, Universidad del Norte, Barranquilla, Colombia.

[2] Departement Fysica, Universiteit Antwerpen, Groenenborgerlaan 171, B-2020 Antwerpen, Belgium.

[3] Departamento de Física, Universidad Nacional de Colombia, Santafé de Bogotá, Colombia.

E-mail: alvarogonzalez@uninorte.edu.co, wlopez@uninorte.edu.co, rhernandezj@uninorte.edu.co, jarodriguezm@bt.unal.edu.co, milorad.milosevic@antwerpen.be, francois.peeters@antwerpen.be

**Abstract.** 2D-GaAs bandgap nature and graphene opening bandgap have been investigated in unexplored Graphene/GaAs bilayer van der Waals heterostructure under both uniaxial stress along c axis and different planar strain distributions using a 551/331 supercell geometry by DFT-VdW-Tkatchenko-Scheffler method and spin-orbit coupling. The 2D-GaAs bandgap nature changes from Γ-$K$ indirect in isolated monolayer to Γ-Γ direct in Graphene/GaAs bilayer heterostructure. In the same latter physical conditions, the graphene displays a bandgap of 5.0 meV. The uniaxial stress strongly influences the graphene electronic bandgap. Symmetrical in-plane strain does not open the graphene bandgap. Nevertheless, it induces remarkable changes on the GaAs width around the Fermi level. However, when applying asymmetrical in-plane strain to graphene/GaAs, the graphene sublattice symmetry is broken, and the graphene bandgap is open at the Fermi level to a maximum width of 814 meV. This value is much higher than that reported for graphene under asymmetrical strain. The Γ-Γ direct nature of GaAs remains unchanged in Graphene/GaAs under different types of applied strain. Phonon dispersion and elastic constants analysis display the dynamical and mechanical stability of Graphene/GaAs system, respectively. The calculated mechanical properties for bilayer heterostructure are better than those of their constituent monolayers. This latter finding, together with the tunable graphene bandgap not only by the strength but also by the direction of the strain, feature the likelihood of enhancing the physical characteristics of potential graphene-based group-IIIV electronic devices by strain engineering.

Submitted to: *J. Phys.: Condens. Matter*

*Keywords*:Density Functional Theory, graphene, field effect transistor, tunable, heterostructure, two dimensional gallium arsenide.

## 1. Introduction

The unique physical properties of two-dimensional graphene related materials (2D-GRM), such as low dimensionality, flexibility, high mechanical strength, lightness, in-plane covalent bonding and dangling-bond-free lattice, allow them a variety of potential applications, for instance: catalysis, biomedicine, conductive ink, sensors, coating, light emitting devices, composites, storage and production of energy, touch panels and high frequency electronics, among others [1–8]. Therefore, during the last ten years, the scientific community has developed an intense research on 2D nanomaterials, e.g., graphene [9], X-enes (X = B, Si, Ge, Sn, P, Bi) [10–18], X-anes (Graphane, Silicane, Germanane, Stanane) [19, 20], fluro-X-enes [20], MXenes [21], IIIV systems [22–27], transition metal dichalcogenides (TMDs) [28–31], layered oxides [32], layered double hydroxides (LDHs) [33], metal-organic frameworks (MOFs) [34,35], covalent organic frameworks (COFs) [36], polymers [37–39] and metals [40–43].

Recently, theoretical and experimental research have focused on the study of van der Waals heterostructures by controlled multi-stacking of diverse layering materials such as metals, semiconductors or insulators [1,44–46]. These novel materials will display interesting structural, electronic, optical and mechanical properties different from those of the 2D materials they are built of. Hence, they can be used to design new electronic and optoelectronic devices with unprecedented features or unique functionalities, such as tunnelling transistors, barristors, flexible electronics, photodetectors, photovoltaics and light-emitting devices [46]. Due to the astonishing physical properties of graphene, e.g., its electrons display ballistic charge carriers transport, graphene is likely the most common component in future van der Waals graphene-based electronic devices [47]. Unfortunately, graphene lacks a bandgap, which is essential for controlling the conductivity by electronic means [48].

The absence of a gap in graphene, together with the linear dispersion of the bands at $K$ point and the equivalence of the two carbon sublattices, restrains the Dirac fermions from getting a finite mass, which constrains the use of graphene in electronic devices. The importance of inducing a bandgap in graphene relies on generating an effective mass for the Dirac fermions, which offers the potential to improve the characteristics of graphene-based field effect transistors (FETs) [49]. This bandgap drawback has motivated Scientists to look for new 2D-materials beyond graphene. It has been found in these studies that graphene bandgap can be modulated by adsorption of H and F [20, 48], and by graphene-based heterostructures [44, 45, 50, 51]. Due to the strain can modify the interatomic distances and relative positions of atoms within a material, the electronic structure of a heterostructure can be also tuned by applying strain [52]. Among these heterostructures, those with lateral graphene display higher electronic quality [44,45,51].

Graphene-based group IIIV heterostructures have been studied in bilayer [49] and multilayer systems [53, 54] in order to tune the graphene band gap for optoelectronics and optics applications. Giovannetti *et al.* [49] studied graphene on single layer BN system by density functional calculations. They found that the presence of $h$-BN breaks the sublattice symmetry of graphene, inducing a bandgap of 53 $meV$. Direct growth of graphene on $h$-BN and viceversa has been achieved by CVD methods [5,55,56]. Using first principle calculations, Kaloni *et al.* [53] predicted finite and tunable bandgaps for superlattices in which a single graphene layer alternates with *h*-BN slabs of variable thickness. In addition, heterostructures where one, two or more graphene (other 2D-systems) layers sandwiched between two other 2D-systems (graphene) have been studied [54, 57, 58].

The following scientific findings motivated us to carry out this study:

i) There are some pioneer studies [59, 60] indicating splitting of electron and hole energy bands by spin-orbit coupling (SOC) in 2D-GaAs heterostructures. Rashba *et al.* [61] were motivated by these pioneer 2D studies to investigate the SOC contribution to the electron Hamiltonian, a term currently known as the Rashba term.

ii) Recently, 2D *h*-GaAs has been reported as a mechanical and dynamically stable semiconductor by first-principles studies [24, 25].

iii) Theoretical and experimental studies state the importance of graphene-based group III−V heterostructures to modulate the band gap of graphene for electronic applications [5, 49, 53–58].

iv) There is some theoretical and experimental research that highlight the importance of Graphene/GaAs systems for future practical applications in plasmonic and photonic technology [62–66]

v) To the best of our knowledge, there are no previous studies about tuning the bandgap in Graphene/GaAs bilayer heterostructures.

In this paper, we study first the structural properties and dynamical stability of Graphene/GaAs bilayer heterostructure. Then, its electronic and mechanical properties and, finally, the effect of both uniaxial stress along c axis and different planar strain distributions on the electronic properties of Graphene/GaAs. This research has been carried out using vdW-Tkatchenko-Scheffler (DFT-TS) method [67] and SOC within DFT framework [68, 69]. Our results predict a novel 2D graphene-based heterostructure for potential electronic applications.

## 2. Computational and theoretical details

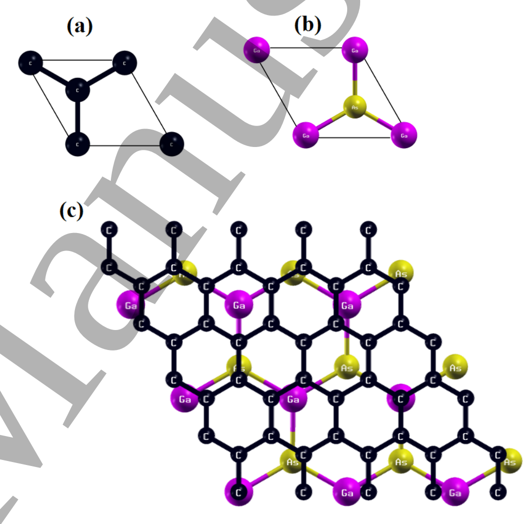


**Figure 1.** (Color online) Honeycomb unit cells for (a) Graphene, (b) 2D-GaAs monolayers, and (c) 551-Graphene/331 GaAs bilayer crystal heterostructure.

The calculations were performed using *vienna ab-initio simulation package* (`VASP`) [70, 71] employing the first principles pseudopotential method in the framework of the DFT [68, 69]. VdW-Tkatchenko-Scheffler (DFT-TS) method [67] and the spin-orbit coupling (SOC) have also been taken into account in our calculations. Exchange and correlation effects were treated with generalized gradient approximation (GGA) implemented in the Perdew-Burke-Ernzerhof functional (PBE) [72]. The core electrons

**Table 1.** Calculated lattice constant ($a$ (Å)), angle between neighboring bonds ($\theta$), Planar (PL) or Low-Buckled (LB) geometry (G),buckling parameter ($\Delta$ (Å)),nearest-neighbor distance ($d$), interlayer distance ($d_L$ ), and bandgap value ($E_G$) for 2D grapgene and GaAs monolayers, and graphene and GaAs in 551-Graphene/331-GaAs bilayer heterostructure.

| | $a$ (Å) | $\theta$ | G | $\Delta$ (Å) | $d$ (Å) | $d_L$ (Å) | $E_G$ ($eV$) |
|---|---|---|---|---|---|---|---|
| **Graphene** | 2.465<br>2.460 [25] | 120<br>120 [25] | PL<br>PL [25] | 0<br>0 [25] | 1.423<br>1.420 [25] | -<br>- | 0<br>0 [25] |
| **2D-GaAs** | 4.048<br>4.050 [24]<br>3.970 [25] | 114.4<br>114.3 [24]<br>114.7 [25] | LB<br>LB [24]<br>LB [25] | 0.577<br>0.550 [24]<br>0.550 [25] | 2.407<br>2.410 [24]<br>2.380 [25] | - | 1.03 $\Gamma K$<br>1.08 $\Gamma K$ [24]<br>1.29 $\Gamma K$ [25] |
| **551-Graphene/ 331-GaAs** | | | | | | | |
| **Graphene** | 2.459 | 120 | PL | 0.001 | 1.419 | 3.476 | 0.049 $KK$ |
| **GaAs** | 4.091 | 115.8 | L.B | 0.501 | 2.427 | - | 0.729 $\Gamma\Gamma$ |

were described by the projector augmented wave (PAW) method [73, 74] wherein the $d$ states for Ga and As were included as valence electrons in their PAW pseudo-potentials. The valence electron configurations for C, Ga and As are considered as $2s^2 2p^2$, $3d^{10}4s^2 4p^1$ and $3d^{10}4s^2 4p^3$, respectively. The hexagonal primitive cell, with one Ga atom and one As atom, see Figure 1(b), was constructed from the zinc-blende structure in the (111) plane [24]. In order to reduce the missmatch between graphene and 2D-GaAs hexagonal monolayers in Graphene/2D-GaAs bilayer heterostructure, a 551/331 supercell geometry has been used in this study, as shown in Figures 1(a), 1(b) and 1(c), respectively. The electron wave function was expanded in plane waves up to a cutoff energy of 500 eV for all the calculations. A gamma-centered grid of 25×25×1 $k$-point has been used to sample the irreducible Brillouin zone in the Monkhorst-Pack special scheme [75] for calculations, except for 551-Graphene/331-GaAs bilayer heterostructure where a 8×8×1 $k$-point was used. Phonon calculations have been performed by taking into account the interactions in a 10×10×1-Graphene/6×6×1-GaAs supercell [76]. The PYPROCAR code was used to plot the electronic bands of Graphene/GaAs bilayer heterostructure [77]. In addition, a 20 Å vacuum spacing between the adjacent supercells is kept to avoid interactions. The optimized parameters for graphene, 2D-GaAs monolayers, and 551-Graphene/331-GaAs bilayer heterostructure are depicted in Table 1. Stress-based approach is implemented [78,79] to study the mechanical properties. The elastic tensor is determined by performing finite distortions of the optimized lattice and deriving the elastic constants from the strain-stress relationship (Hooke's law) [78, 79].

In our study, the spin-orbit interaction for 551-Graphene/331-GaAs bilayer heterostructure has been taken into account. Spin-orbit coupling is a relativistic interaction between moving electrons with $\mathbf{v}$=$\mathbf{p}$/m and a local electric field $\mathbf{E}= -\frac{1}{q}\frac{dV(r)}{dr}\frac{\mathbf{r}}{r}$ in their rest frame created by the proton, where $\mathbf{q}$ is the charge of the moving electrons and V(r)=$-\frac{e^2}{r}$ is the electro-

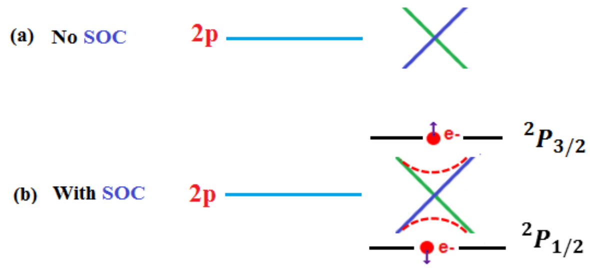


**Figure 2.** (Color online) Orbital angular momentum of *p*-graphene state ($l$=1) with (a) no coupling and (b) coupling with its spin intrinsic momentum

static energy of the electron. Special relativity indicates that then appears, in the electron frame, a magnetic field, described by [80]

$$\mathbf{B} = -\frac{1}{c^2}(\mathbf{v} \times \mathbf{E}) \quad (1)$$

where $\mathbf{B}$ is equivalent to:

$$\mathbf{B} = -(\frac{e^2}{qm_e c^2 r^3})\mathbf{L} \quad (2)$$

where $\mathbf{L} = \mathbf{r}\times\mathbf{P}$ represents the electron orbital angular momentum. Due to the interaction of $\mathbf{B}$ with the electron intrinsic magnetic moment $\mathbf{Ms}$, given by:

$$\mathbf{Ms} = \frac{q}{m_e}\mathbf{S} \quad (3)$$

and by Zeeman effect, the orbital energy levels are splitting, which can lead to different transition levels with energy:

$$H_{so} = -\mathbf{Ms}\cdot\mathbf{B} \quad (4)$$

From equations (2), (3) and (4), $H_{so}$ can be rewritten by:

$$H_{so} = \xi(r)\mathbf{L}\cdot\mathbf{S} \quad (5)$$

where $\xi$ (r)= $e^2/2m^2{}_e c^2$r$^3$ contains the entire radial dependence of the SOC Hamiltonian operator [81]. The factor 1/2 is due to the fact that the electron spin rotates with respect to the laboratory reference frame [80]. $\mathbf{L}$ and $\mathbf{S}$ are the electron orbital and spin angular momentum, respectively. When the orbital angular momentum of *p*-graphene orbital interacts with its spin intrinsic momentum, the electron states can be either 3/2 ($^2P_{3/2}$) or 1/2 ($^2P_{1/2}$), depending on the case if $\mathbf{L}$ and $\mathbf{S}$ are parallel or antiparallel, respectively, as shown in Figure 2(b).

The special relativity theory states that for electrons with large average speeds the mass increases, while the radius decreases. In the weakly relativistic domain, the SOC effect is specially noticed for massive atoms of periodic table. There are some pioneer studies [59, 60] indicating splitting of electron and hole energy bands by spin-orbit coupling (SOC) in 2D-GaAs heterostructures. Pyykk*ö* [82] compared the relativistic (Dirac) and nonrelativistic (Schrodinger) dynamics for the valence electron in a given atomic potential, to study the importance of the direct relativistic effect on atomic orbitals. They found a relativistic radial contraction and energetic stabilization for *s* and *p* shells, spin-orbit splitting and the relativistic radial expansion and energetic destabilization of the *d* and all *f* outer shells. They also reported that all three effects were of the same order of magnitude and grow roughly like $Z^2$.

In order to study some mechanical properties that give physical insights into the potential aplications of 551-Graphene/331-GaAs bilayer heterostructures in engineering science, we calculated its $C_{11}$, $C_{12}$, $C_{22}$ and $C_{66}$ elastic constants. Due to hexagonal symmetry, $C_{11} = C_{22}$ and $(C_{11} - C_{12})/2 = C_{66}$ , only two independent elastic constants $C_{11}$ and $C_{12}$ are considered in the stress-strain relation for a 2D hexagonal estructure. Therefore, the Hooke's law ($\sigma_i$ = $C_{ij}$ $\epsilon_j$, where $\sigma_i$ and $\epsilon_j$, i and j are integers, represent the stress and strain, respectively) for 2D hexagonal materials can be expressed in the matrix form [83]:

$$\begin{pmatrix} \sigma_1 \\ \sigma_2 \\ \sigma_3 \end{pmatrix} = \begin{pmatrix} C_{11} & C_{12} & 0 \\ C_{12} & C_{11} & 0 \\ 0 & 0 & \frac{C_{11}-C_{12}}{2} \end{pmatrix} \begin{pmatrix} \epsilon_1 \\ \epsilon_2 \\ \epsilon_3 \end{pmatrix}$$

The Poison's ratio $\nu$, the in-plane Young's modulus $Y_s$, the 2D layer modulus $B_{2D}$ and shear $G_V$ modulus are obtained, from the calculated $C_{11}$ and $C_{12}$ elastic constants, and multiplied later by the corresponding optimized unit-cell $z$ distance. Their respective equations are [84, 85]:

$$\nu = C_{12}/C_{11} \tag{6}$$

$$Y_s = (C_{11}^2 - C_{12}^2)/C_{11} \tag{7}$$

$$B_{2D} = (C_{11} + C_{12})/2 \tag{8}$$

$$G = (C_{11} - C_{12})/2 \tag{9}$$

The calculated elastic constants and the above mentioned mechanical properties for graphene and 2D-GaAs monolayers, and 551-Graphene/331-GaAs bilayer heterostructure are depicted in Table 2. The Poisson's ratio represents the plasticity of the material, the 2D layer modulus gives physical insight about the resilience of a material to stretching, and the shear and in-plane Young's moduli indicate the 2D structure stiffness. Gonzalez *et al* [24] reported for 2D *h*-IIIAs binary compounds that as moved down on the group of elements of the periodic table, the bond length between the neighboring cation-anion atoms increases and the materials display less stiffness and more plasticity.

## 3. Results and discussion

### 3.1. Structural properties and dynamical stability

Honeycomb unit cells for graphene and 2D-GaAs monolayers are shown in Figures 1(a) and 1(b). Graphene monolayer displays a planar geometry while 2D-GaAs presents a buckled one. The TS-vdW optimized parameters for graphene and 2D-GaAs hexagonal monolayers, as well as for graphene and 2D-GaAs in 551-Graphene/331-GaAs bilayer heterostructures (Figure 1(c)), are shown for comparison in Table 1. Our results for 2D-GaAs and graphene monolayers are in good agreement with previous theoretical ones reported by DFT. The lattice parameter value of graphene monolayer is 39.1 % shorter than that of 2D-GaAs monolayer. Using a computational method Kumar *et al* reported that lattice mismatch between two different bilayers causes elastic strains, which significantly affects their electronic properties [86]. In order to reduce this mismatch, a 551-Graphene and 331-GaAs geometries were chosen. These selected geometries reduced the mismatch to 1.49 % between 551-Graphene and 331-GaAs sheets.

The vdW interlayer interaction between 551-graphene and 331-GaAs layers reduces the laticce constant of graphene by 0.24 % and increases that of the GaAs by 1.01 % compared to the respective ones from pristine monolayers. As a result, the initial mismatch between 551-Graphene and 331-GaAs is reduced from 1.49 % to 0.18 %, which increases the mechanical and dynamical stability of our system, as will be shown in the next sections. The optimized DFT-TS interlayer spacing ($d_L$) between 551-graphene and 331-GaAs sheets is 3.476 Å. This value is higher than that found for graphene-BN bilayer, 3.34 Å [49], and reasonably comparable to that of 551-graphene/441-Mo$S_2$ heterostructures, 3.40 Å [87]. The interlayer distance is sensible to the vdW flavour used in the calculatations. So, it is of vital importance the correct vdW flavour

**Table 2.** Calculated 2D Poissons ratio ($\nu$); Young's ($Y_s$), layer ($B_v$) and Shear ($G_v$) moduli for 2D graphene and GaAs monolayers, and 551-Graphene/331-GaAs bilayer heterostructure.

| | $C_{11}$ (J/m$^2$) | $C_{12}$ (J/m$^2$) | $\nu$ | $Y_S$ (J/m$^2$) | $B_{2D}$ (J/m$^2$) | $G_V$ (J/m$^2$) |
|---|---|---|---|---|---|---|
| **Graphene** | 352.8<br>352.7 [85] | 62.8<br>60.9 [85] | 0.18<br>0.17 [85] | 341.7<br>342.2 [85] | 207.8<br>206.6 [85] | 145.0<br>145.9 [85] |
| **2D-GaAs** | 49.6<br>- | 16.1<br>- | 0.32<br>0.35 [25] | 44.4<br>48.0 [25] | 32.9<br>- | 17.1<br>- |
| **551-Graphene/ 331-GaAs** | 384.7 | 70.0 | 0.18 | 372.1 | 227.4 | 157.0 |

choice [87]. Singh *et al.* reported that the Tkatchenko-Scheffler method effciently evaluates the long-range vdW interactions and accurately predicts interlayer spacing between 551-graphene and 441-Mo$S_2$ sheets [87]. Their reported interlayer distance agrees with the experimental one (3.40 Å) [88]. On the other hand, theoretical [25, 26] and experimental [27] research has predicted and validated the stability of 2D buckled single layer of group III−V with ionicity. Al Balushi *et al.* experimentally reported that graphene plays a critical role in stabilizing ionic 2D buckled group III−V structure. Their results provide a foundation for the discovery and stabilization of 2D group III−V materials that are difficult to prepare via traditional synthesis [27]. Using Bader analysis [89], we found a charge transference of 5.3 electrons from Ga to As for 551-Graphene/331-GaAs bilayer heterostructure, indicating a significant ionicity in the interplanar binding. However, it was not found charge transference from Ga to C atoms.

Figure 3 depicts the calculated phonon dispersion curves for the 551-Graphene/331-GaAs bilayer heterostructure. We can see that the 551-Graphene/331-GaAs system can

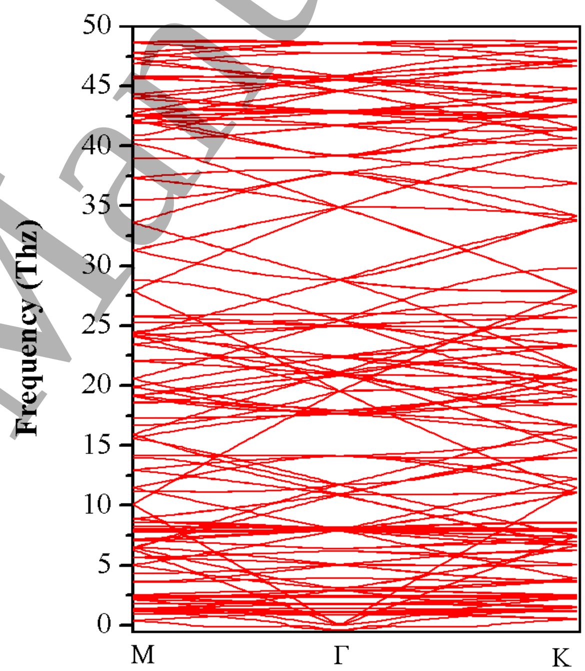


**Figure 3.** (Color online) Phonon dispersion curves for the 551-Graphene/331-GaAs bilayer heterostructure

be stable, because there are no imaginary frequencies in the phonon dispersion. Some few negative frequencies near Γ point are shown. This feature has been found in other 2D-systems [33, 87, 90–92] and highlights the flexural acoustic mode of 2D-systems. They are often present in the theoretical calculations due to inadequate numerical convergence close to Γ point [87].

### *3.2. Electronic structure and Mechanical properties*

The TS-vdW + SOC electronic band structure for the 551-graphene/331-GaAs (X=0.0%) is displayed in Figure 4. The brown lines represent the contributions of Ga-4$s$ and As-4$p_z$ orbitals, while the green one the contribution of C-2$p_z$ orbitals. We can see the semiconductor Γ-Γ direct nature for 331-GaAs layer, with a bandgap size of 0.72 eV, and a near semimetallic nature of 5.0 meV at K point for 551-graphene layer. This electronic behavior for 331-GaAs (Γ-Γ direct) is different from that one reported for 2D-GaAs monolayer (Γ-$K$ indirect) [24, 25]. Thus, the presence of graphene on GaAs layer induces an indirect to direct bandgap transition on GaAs layer, which makes it potential candidate for optoelectronic applications and field-effect transistors. This bandgap transition can be physically explained by the vdW interaction between the localized C-2$p_z$ and As-4$p_z$ orbitals at $K$ point, which shifts this latter orbital downward of the VBM. Singh *et al.* [87] reported that Mo$S_2$ undergoes a direct to indirect (direct) bandgap transition in 441-graphene/331-Mo$S_2$ (551-graphene/441-Mo$S_2$) bilayer heterostructure. Authors state that these bandgap transitions, when changing the layer geometries, are imposed by the level of strain intensity between the layers. Lattice mismatch between two different bilayers causes elastic strains, which significantly affects their electronic properties [86]. The change from indirect to direct of 2D-GaAs bandgap nature is physically important because heterostructures can present high photoluminescence [87]. On the other hand, we found that the proximity effects of GaAs and SOC open a bandgap of 5.0 $meV$ at Dirac point in graphene for Graphene/GaAs. Our result agrees with those found for graphene/BN. It has been reported that strain opens the graphene/BN bandgap in the range of 4 meV to 14 meV [93, 94]. Sing *et al.* found that the SOC and proximity effects of Mo$S_2$ open a direct band gap in graphene of 0.4 meV and 1.1 meV for different Graphene/Mo$S_2$ geometries [87].

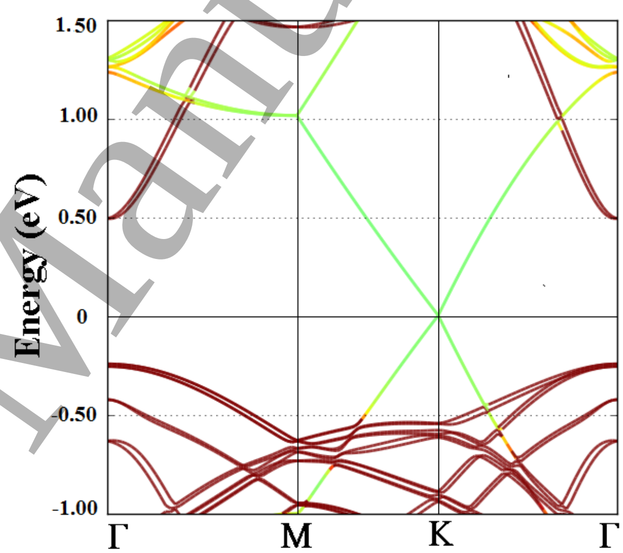


**Figure 4.** (Color online) Electronic band structure for the 551-Graphene/331 GaAs bilayer crystal heterostructure (X=0.0 %). The brown lines represent the contributions of Ga-4$s$ and As-4$p_z$ orbitals, while the green one the contribution of C-2$p_z$ orbitals. The inset displays the bangap opening at Dirac point for graphene.

The elastic constants for graphene and 2D-GaAs monolayers, as well as for 551-Graphene/331-GaAs bilayer system, are tabulated in Table 2. Our results for the monolayer constituents of Graphene/GaAs are in excellent agreement with those reported in previous theoretical and experimental studies. It

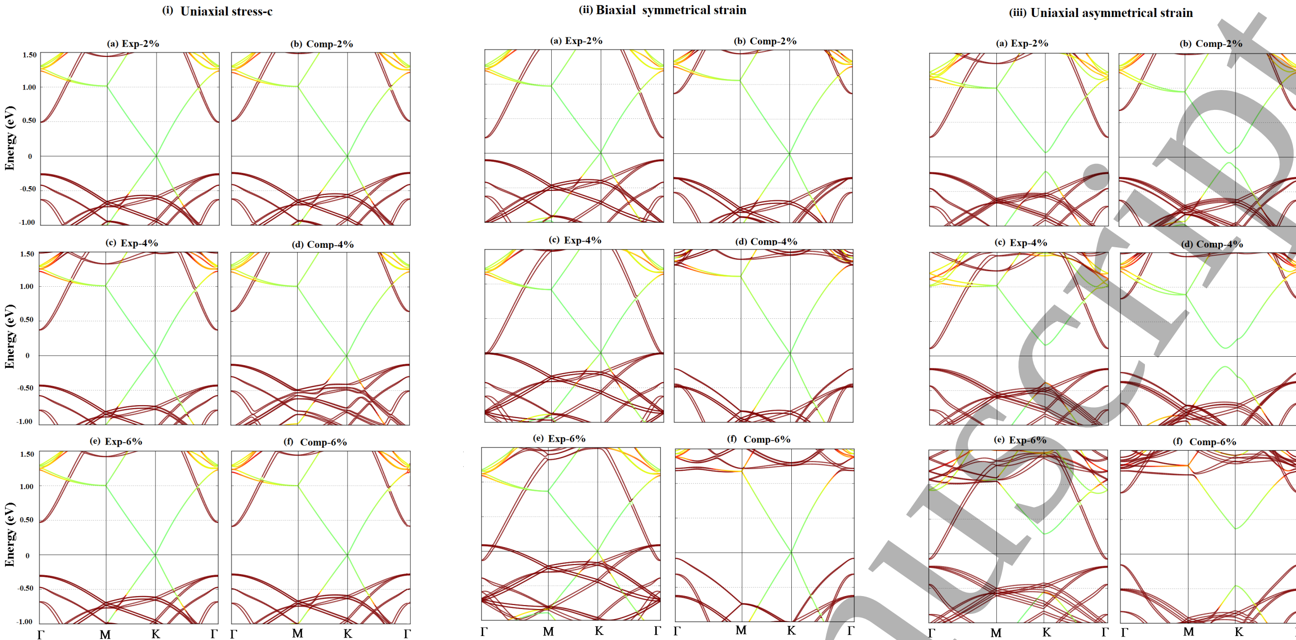


**Figure 5.** (Color online) Electronic structures for i) Uniaxial stress along c−axis ii) Biaxial symmetrical strain and iii) Uniaxial asymmetrical strain along perpendicular C−C bond for X =−6.0%, −4.0%, −2.0 %, +2.0 %, +4.0% and +6.0 % configurations of 551-Graphene/331 GaAs bilayer crystal heterostructure.

is noteworthy that $C_{11}>0$ and $C_{11}-C_{12}>0$, which means that all our systems satisfy the Born stability criteria [95] for mechanically stable 2D hexagonal structures. The calculated Poisson's ratio for 551-Graphene/331-GaAs bilayer system is lesser (equal) than that of 2D-GaAs (graphene) monolayer. On the contrary, the 2D Young's ($Y_s$), layer ($B_{2D}$) and Shear ($G_V$) moduli for bilayer heterostructure are higher when compared to those of their constituent monolayer. Therefore, 551-graphene/331-GaAs is a stronger material than graphene but with its same plasticity, which makes it attractive for potential applications in engineering science.

### *3.3. Tuning Graphene and 2D-GaAs bandgaps*

Stress applied on heterostructure materials changes the interatomic distances and the relative positions of the atoms, which influences the electronic structure with potential optical applications [96]. Therefore, we have investigated the impact on the electronic properties of graphene and GaAs in graphene/GaAs bilayer hetrostructure under uniaxial stress along c axis and different planar strain distributions.

In order to study the effect of uniaxial stress along *c* axis on electronic properties of 551-Graphene/331-GaAs bilayer crystal heterostructure, the equilibrium interlayer distance between 551-Graphene and 331-GaAs layers was modified by X =−6.0%, −4.0%, −2.0%, +2.0%, +4.0% and +6.0%. During each expansion (X>0) and compression (X< 0) process, the vertical coordinate was kept fixed at each separation while atoms were allowed to relax in the plane of layers. Figure 5(i) displays the electronic structures for all these configurations. For X= +2.0%, +4.0% and +6.0% expansion cases, the 551-Graphene bandgap (331-GaAs) is opened by 26.0% (4.2%), 68.0% (8.3%) and 68.0% (5.6%).

For the uniaxial compression along *c* axis, the graphene (GaAs) bandgap increases from 7.3 meV (0.75 eV) to 9.4 meV (0.78 eV) as the strain increases from −2.0% to −4.0% before decreasing to 5.2 meV (0.67 eV) for −6.0%. From the results found for the uniaxial strain along *c* axis, we can infer that interlayer distance plays an important role for tuning both the graphene and GaAs bandgap in Graphene/GaAs bilayer heterostructure. The graphene bandgap opening could be attributed to the enhanced SOC of graphene due to proximity of the GaAs-bukcled effective potential. Using first-priciples method, Youngbin *et al.* [52] studied the effect of strain on the bandgap characteristics of MXene semiconducting for useful optical devices. They reported that this material experiences an indirect to direct band gap transition with variation of the bandgap size at a relatively small critical strain of about 2%.

For the symmetrical strain distribution, the system undergoes in-plane biaxial stretching and compression of 2.0%, 4.0% and 6.0% from its optimized lattice parameter value. Then, the lattice structure was optimized, the lattice vectors were set to be fixed at their strained values while only the atomic coordinates were allowed to relax. Figure 5(ii) shows the band structure of the graphene/GaAs systems with X= −6.0%, −4.0%, −2.0%, +2.0%, +4.0% and +6.0% for symmetrical strain. We find that there is no bandgap opening around the Fermi level for the graphene with any strength of symmetrical tensile or compressive strain. Nevertheless, strain results in remarkable change of the GaAs bandgap width around the Fermi level. As shown in Figure 5(ii), strain results in decrease in the GaAs bandgap width until becoming metallic, while compressive strain leads to increase in the GaAs bandgap width.

In the asymmetrical strain distribution, graphene/GaAs bilayer supercell undergoes uniaxial stretching and compression in one direction, perpendicular to C−C bonds, of 2%, 4% and 6% from its optimized lattice parameter value, and unstrained along the other direction. Figure 5(iii) displays the electronic structures for X= −6.0%, −4.0%, −2.0%, +2.0%, +4.0% and +6.0% configurations. For X=+2.0% and +4.0%, the 551-Graphene bandgap (331-GaAs) is opened (narrowed) 267 and 541 meV (0.502 and 0.286 eV). As the expansion is increased to +6.0% the system becomes slightly metallic. For X=+2% and +4%, the graphene has a bandgap located at the left side of K point; while for 6%, at K point. Gui *et al.* found similar results for asymmetrical strain distributions in graphene, though they reported direct and indirect graphene bandgap nature depending on the compression value [97].

On the other hand, Figure 5(iii) displays that the graphene (GaAs) bandgap width increases to 91 (0.95), 248 (1.05) and 814 (1.04 eV) meV for X= −2.0% , −4.0% and −6.0%, respectively. We can also notice that GaAs bandgap keeps its direct nature at Γ point. Gui *et al.* reported that for the asymmetrical strain distribution perpendicular to C−C bonds in graphene, the bandgap increases from 0 to 170 meV as the strain increases to 4.91% before decreasing [97]. The authors reported that the lattice symmetry breaking results in graphene bandgap opening at the Fermi level. From Figure 5(iii) is noticed that the valence-band maximum for GaAs is shifted upward, closer to the Fermi level as the compression increases, while the graphene valence-band maximum is shifted downward, farther from the Fermi level. One physical reason for this is that as the compression reaches a value larger than 4%, the repulsion between the charge accumulation around C atoms becomes stronger so the *p*-C orbitals are shifted downward farther from the Fermi level. For the case of GaAs, as the compression increases, due to the electronegative difference between their atoms, the attraction between the charge accumulation around Ga and As atoms becomes stronger so the GaAs orbitals are shifted near each other.

From the above mentioned results, obtained for the symmetrical and asymmetrical strain applied to graphene/GaAs system, we can conclude that the nature for both GaAs and graphene electronic band structures depends on its lattice symmetry. The lattice symmetry breaking results in graphene bandgap opening at the Fermi level. Our findings are important to tune the electronic properties of 551-graphene/331-GaAs heterostructure by strain engineering for potential optical aplications.

## 4. Conclusions

DFT-VdW-Tkatchenko-Scheffler method and spin-orbit coupling have been used to investigate the physical effects on electronic band structures of 2D-GaAs and graphene monolayer constituents in Graphene/GaAs bilayer heterostructure using a 551/331 supercell geometry. It was found that 2D-GaAs bandgap nature changes from $\Gamma-K$ indirect in isolated monolayer to $\Gamma-\Gamma$ direct in bilayer heterostructure. This bandgap transition can be physically explained by the vdW interaction between the localized C-2$p_z$ and As-4$p_z$ orbitals at $K$ point, which shifts this latter orbital downward of the VBM. The uniaxial stress along c-axis strongly influences the graphene electronic bandgap. The interlayer distance plays an important role for tuning both the graphene and GaAs bandgap in Graphene/GaAs bilayer heterostructure. The graphene bandgap opening could be attributed to the enhanced SOC of graphene due to proximity of the GaAs-bukcled effective potential. $\Gamma-\Gamma$ direct band gap of 2D-GaAs in 551-Graphene/331-GaAs is not altered as varying distance interlayer. These are extremely important findings for potential optical applications by strain engineering. Symmetrical in-plane strain does not open the graphene bandgap. Nevertheless, it induces remarkable changes on the GaAs width around the Fermi level. When applying asymmetrical in-plane strain to graphene/GaAs, the graphene sublattice symmetry is broken, and the graphene bandgap is open at the Fermi level to a maximum width of 814 meV. We can conclude that the nature for both GaAs and graphene electronic band structures depends on its lattice symmetry. The lattice symmetry breaking results in graphene band-gap opening at the Fermi level. Our findings are important to tune the electronic properties of 551-graphene/331-GaAs heterostructure by strain engineering for potential optical aplications. Phonon dispersion and elastic constants analysis display, respectively, the dynamical and mechanical stability of 551-Graphene/331-GaAs bilayer vdW-heterostructure. The calculated 2D Young's ($Y_s$), layer ($B_{2D}$) and Shear ($G_V$) moduli for bilayer heterostructure are higher than those of its monolayer constituents, which indicates that our studied bilayer material displays more in-plane stiffness than its monolayer constituents. Our findings feature the likelihood of enhancing the physical characteristics of potential graphene-based group-IIIV optoelectronic devices by science engineering.

## Conflicts of interest

There are no conflicts to declare.

## Acknowledgements

This work has been carried out by the financial support of Universidad del Norte and Colciencias (Administrative Department of Science, Technology and Research of Colombia) under Convocatoria 712 - Convocatoria para proyectos de investigación en Ciencias Básicas, año 2015, Cod: 121571250192, Contrato 110-216. The authors also acknowledge the support from the High Performance Computing core facility CalcUA (HPC) at the University of Antwerp, Belgium.

## References

[1] Andrea C Ferrari, Francesco Bonaccorso, Vladimir Fal'Ko, Konstantin S Novoselov, Stephan Roche, Peter Bøggild, Stefano Borini, Frank HL Koppens, Vincenzo Palermo, Nicola Pugno, et al. Science and technology roadmap for graphene, related two-dimensional crystals, and hybrid systems. *Nanoscale*, 7(11):4598–4810, 2015.

[2] Fang Song and Xile Hu. Exfoliation of layered double hydroxides for enhanced oxygen evolution catalysis. *Nature communications*, 5:4477, 2014.

[3] Mark A Lukowski, Andrew S Daniel, Fei Meng, Audrey Forticaux, Linsen Li, and Song Jin. Enhanced hydrogen evolution catalysis from chemically exfoliated metallic mos2 nanosheets. *Journal of the American Chemical Society*, 135(28):10274–10277, 2013.

[4] Yu Chen, Chaoliang Tan, Hua Zhang, and Lianzhou Wang. Two-dimensional graphene analogues for biomedical applications. *Chemical Society Reviews*, 44(9):2681–2701, 2015.

[5] Zheng Liu, Yongji Gong, Wu Zhou, Lulu Ma, Jingjiang Yu, Juan Carlos Idrobo, Jeil Jung, Allan H MacDonald, Robert Vajtai, Jun Lou, et al. Ultrathin high-temperature oxidation-resistant coatings of hexagonal boron nitride. *Nature communications*, 4:2541, 2013.

[6] F Schedin, AK Geim, SV Morozov, EW Hill, P Blake, MI Katsnelson, and KS Novoselov. Detection of individual gas molecules adsorbed on graphene. *Nature materials*, 6(9):652, 2007.

[7] Chaoliang Tan, Zhengdong Liu, Wei Huang, and Hua Zhang. Non-volatile resistive memory devices based on solution-processed ultrathin two-dimensional nanomaterials. *Chemical Society Reviews*, 44(9):2615–2628, 2015.

[8] Muharrem Acerce, Damien Voiry, and Manish Chhowalla. Metallic 1t phase mos 2 nanosheets as supercapacitor electrode materials. *Nature nanotechnology*, 10(4):313, 2015.

[9] Andre K Geim and Konstantin S Novoselov. The rise of graphene. In *Nanoscience and Technology: A Collection of Reviews from Nature Journals*, pages 11–19. World Scientific, 2010.

[10] Alessandro Molle, Joshua Goldberger, Michel Houssa, Yong Xu, Shou-Cheng Zhang, and Deji Akinwande. Buckled two-dimensional xene sheets. *Nature materials*, 16(2):163, 2017.

[11] Zachary A Piazza, Han-Shi Hu, Wei-Li Li, Ya-Fan Zhao, Jun Li, and Lai-Sheng Wang. Planar hexagonal b 36 as a potential basis for extended single-atom layer boron sheets. *Nature communications*, 5:3113, 2014.

[12] Boubekeur Lalmi, Hamid Oughaddou, Hanna Enriquez, Abdelkader Kara, Sébastien Vizzini, Bénidicte Ealet, and Bernard Aufray. Epitaxial growth of a silicene sheet. *Applied Physics Letters*, 97(22):223109, 2010.

[13] Patrick Vogt, Paola De Padova, Claudio Quaresima, Jose Avila, Emmanouil Frantzeskakis, Maria Carmen Asensio, Andrea Resta, Bénédicte Ealet, and Guy Le Lay. Silicene: compelling experimental evidence for graphenelike two-dimensional silicon. *Physical review letters*, 108(15):155501, 2012.

[14] Cheng-Cheng Liu, Hua Jiang, and Yugui Yao. Low-energy effective hamiltonian involving spin-orbit coupling in silicene and two-dimensional germanium and tin. *Physical Review B*, 84(19):195430, 2011.

[15] Bas van den Broek, Michel Houssa, Emilio Scalise, Geoffrey Pourtois, VV Afanas'ev, and Andre Stesmans. Two-dimensional hexagonal tin: ab initio geometry, stability, electronic structure and functionalization. *2D Materials*,

1(2):021004, 2014.

[16] Han Liu, Adam T Neal, Zhen Zhu, Zhe Luo, Xianfan Xu, David Tománek, and Peide D Ye. Phosphorene: an unexplored 2d semiconductor with a high hole mobility. *ACS nano*, 8(4):4033–4041, 2014.

[17] Han Liu, Yuchen Du, Yexin Deng, and D Ye Peide. Semiconducting black phosphorus: synthesis, transport properties and electronic applications. *Chemical Society Reviews*, 44(9):2732–2743, 2015.

[18] Yunhao Lu, Wentao Xu, Mingang Zeng, Guanggeng Yao, Lei Shen, Ming Yang, Ziyu Luo, Feng Pan, Ke Wu, Tanmoy Das, et al. Topological properties determined by atomic buckling in self-assembled ultrathin bi (110). *Nano letters*, 15(1):80–87, 2014.

[19] Huabing Shu, Yunhai Li, Shudong Wang, and Jinlan Wang. Quasi-particle energies and optical excitations of hydrogenated and fluorinated germanene. *Physical Chemistry Chemical Physics*, 17(6):4542–4550, 2015.

[20] O Leenaerts, H Peelaers, AD Hernández-Nieves, B Partoens, and FM Peeters. First-principles investigation of graphene fluoride and graphane. *Physical Review B*, 82(19):195436, 2010.

[21] Michael Naguib, Vadym N Mochalin, Michel W Barsoum, and Yury Gogotsi. 25th anniversary article: Mxenes: a new family of two-dimensional materials. *Advanced Materials*, 26(7):992–1005, 2014.

[22] Yi Lin, Tiffany V Williams, and John W Connell. Soluble, exfoliated hexagonal boron nitride nanosheets. *The Journal of Physical Chemistry Letters*, 1(1):277–283, 2009.

[23] Rashid Ahmed, S Javad Hashemifar, Hadi Akbarzadeh, Maqsood Ahmed, et al. Ab initio study of structural and electronic properties of iii-arsenide binary compounds. *Computational materials science*, 39(3):580–586, 2007.

[24] Alvaro González-García, William López-Pérez, J Rivera-Julio, FM Peteers, Víctor Mendoza-Estrada, and Rafael González-Hernández. Structural, mechanical and electronic properties of two-dimensional structure of iii-arsenide (111) binary compounds: An ab-initio study. *Computational Materials Science*, 144:285–293, 2018.

[25] Hasan Şahin, Seymur Cahangirov, Mehmet Topsakal, E Bekaroglu, E Akturk, Ramazan Tuğrul Senger, and Salim Ciraci. Monolayer honeycomb structures of group-iv elements and iii-v binary compounds: First-principles calculations. *Physical Review B*, 80(15):155453, 2009.

[26] A Onen, D Kecik, E Durgun, and S Ciraci. Gan: From three-to two-dimensional single-layer crystal and its multilayer van der waals solids. *Physical Review B*, 93(8):085431, 2016.

[27] Zakaria Y Al Balushi, Ke Wang, Ram Krishna Ghosh, Rafael A Vilá, Sarah M Eichfeld, Joshua D Caldwell, Xiaoye Qin, Yu-Chuan Lin, Paul A DeSario, Greg Stone, et al. Two-dimensional gallium nitride realized via graphene encapsulation. *Nature materials*, 15(11):1166, 2016.

[28] Manish Chhowalla, Hyeon Suk Shin, Goki Eda, Lain-Jong Li, Kian Ping Loh, and Hua Zhang. The chemistry of two-dimensional layered transition metal dichalcogenide nanosheets. *Nature chemistry*, 5(4):263, 2013.

[29] Xiao Huang, Zhiyuan Zeng, and Hua Zhang. Metal dichalcogenide nanosheets: preparation, properties and applications. *Chemical Society Reviews*, 42(5):1934–1946, 2013.

[30] Mingsheng Xu, Tao Liang, Minmin Shi, and Hongzheng Chen. Graphene-like two-dimensional materials. *Chemical reviews*, 113(5):3766–3798, 2013.

[31] Manish Chhowalla, Zhongfan Liu, and Hua Zhang. Two-dimensional transition metal dichalcogenide (tmd) nanosheets. *Chemical Society Reviews*, 44(9):2584–2586, 2015.

[32] Minoru Osada and Takayoshi Sasaki. Exfoliated oxide nanosheets: new solution to nanoelectronics. *Journal of Materials Chemistry*, 19(17):2503–2511, 2009.

[33] Qiang Wang and Dermot O'Hare. Recent advances in the synthesis and application of layered double hydroxide (ldh) nanosheets. *Chemical reviews*, 112(7):4124–4155, 2012.

[34] Yuan Peng, Yanshuo Li, Yujie Ban, Hua Jin, Wenmei Jiao, Xinlei Liu, and Weishen Yang. Metal-organic framework nanosheets as building blocks for molecular sieving membranes. *Science*, 346(6215):1356–1359, 2014.

[35] Tania Rodenas, Ignacio Luz, Gonzalo Prieto, Beatriz Seoane, Hozanna Miro, Avelino Corma, Freek Kapteijn, Francesc X Llabrés i Xamena, and Jorge Gascon. Metal–organic framework nanosheets in polymer composite materials for gas separation. *Nature materials*, 14(1):48, 2015.

[36] John W Colson, Arthur R Woll, Arnab Mukherjee, Mark P Levendorf, Eric L Spitler, Virgil B Shields, Michael G Spencer, Jiwoong Park, and William R Dichtel. Oriented 2d covalent organic framework thin films on single-layer graphene. *Science*, 332(6026):228–231, 2011.

[37] Max J Kory, Michael Wörle, Thomas Weber, Payam Payamyar, Stan W Van De Poll, Julia Dshemuchadse, Nils Trapp, and A Dieter Schlüter. Gram-scale synthesis of two-dimensional polymer crystals and their structure analysis by x-ray diffraction. *Nature chemistry*, 6(9):779, 2014.

[38] Patrick Kissel, Daniel J Murray, William J Wulftange, Vincent J Catalano, and Benjamin T King. A nanoporous two-dimensional polymer by single-crystal-to-single-crystal photopolymerization. *Nature chemistry*, 6(9):774, 2014.

[39] Chaoliang Tan, Xiaoying Qi, Xiao Huang, Jian Yang, Bing Zheng, Zhongfu An, Runfeng Chen, Jun Wei, Ben Zhong Tang, Wei Huang, et al. Single-layer transition metal dichalcogenide nanosheet-assisted assembly of aggregation-induced emission molecules to form organic nanosheets with enhanced fluorescence. *Advanced Materials*, 26(11):1735–1739, 2014.

[40] Zhanxi Fan, Xiao Huang, Chaoliang Tan, and Hua Zhang. Thin metal nanostructures: synthesis, properties and applications. *Chemical science*, 6(1):95–111, 2015.

[41] Xiao Huang, Shaozhou Li, Yizhong Huang, Shixin Wu, Xiaozhu Zhou, Shuzhou Li, Chee Lip Gan, Freddy Boey, Chad A Mirkin, and Hua Zhang. Synthesis of hexagonal close-packed gold nanostructures. *Nature communications*, 2:292, 2011.

[42] Xiaoqing Huang, Shaoheng Tang, Xiaoliang Mu, Yan Dai, Guangxu Chen, Zhiyou Zhou, Fangxiong Ruan, Zhilin Yang, and Nanfeng Zheng. Freestanding palladium nanosheets with plasmonic and catalytic properties. *Nature nanotechnology*, 6(1):28, 2011.

[43] Haohong Duan, Ning Yan, Rong Yu, Chun-Ran Chang, Gang Zhou, Han-Shi Hu, Hongpan Rong, Zhiqiang Niu, Junjie Mao, Hiroyuki Asakura, et al. Ultrathin rhodium nanosheets. *Nature communications*, 5:3093, 2014.

[44] Alexander S Mayorov, Roman V Gorbachev, Sergey V Morozov, Liam Britnell, Rashid Jalil, Leonid A Ponomarenko, Peter Blake, Kostya S Novoselov, Kenji Watanabe, Takashi Taniguchi, et al. Micrometer-scale ballistic transport in encapsulated graphene at room temperature. *Nano letters*, 11(6):2396–2399, 2011.

[45] Cory R Dean, Andrea F Young, Inanc Meric, Chris Lee, Lei Wang, Sebastian Sorgenfrei, Kenji Watanabe, Takashi Taniguchi, Phillip Kim, Kenneth L Shepard, et al. Boron nitride substrates for high-quality graphene electronics. *Nature nanotechnology*, 5(10):722, 2010.

[46] Yuan Liu, Nathan O Weiss, Xidong Duan, Hung-Chieh Cheng, Yu Huang, and Xiangfeng Duan. Van der waals heterostructures and devices. *Nature Reviews Materials*, 1(9):16042, 2016.

[47] Andre K Geim and Irina V Grigorieva. Van der waals heterostructures. *Nature*, 499(7459):419, 2013.

[48] Richard Balog, Bjarke Jørgensen, Louis Nilsson, Mie Andersen, Emile Rienks, Marco Bianchi, Mattia Fanetti, Erik Lægsgaard, Alessandro Baraldi, Silvano Lizzit, et al. Bandgap opening in graphene induced by patterned hydrogen adsorption. *Nature materials*, 9(4):315, 2010.

[49] Gianluca Giovannetti, Petr A Khomyakov, Geert Brocks, Paul J Kelly, and Jeroen Van Den Brink. Substrate-induced band gap in graphene on hexagonal boron nitride: Ab initio density functional calculations. *Physical Review B*, 76(7):073103, 2007.

[50] Abbas Ebnonnasir, Badri Narayanan, Suneel Kodambaka, and Cristian V Ciobanu. Tunable mos2 bandgap in mos2-graphene heterostructures. *Applied Physics Letters*, 105(3):031603, 2014.

[51] SJ Haigh, A Gholinia, R Jalil, S Romani, L Britnell, DC Elias, KS Novoselov, LA Ponomarenko, AK Geim, and R Gorbachev. Cross-sectional imaging of individual layers and buried interfaces of graphene-based heterostructures and superlattices. *Nature materials*, 11(9):764, 2012.

[52] Youngbin Lee, Sung Beom Cho, and Yong-Chae Chung. Tunable indirect to direct band gap transition of monolayer sc2co2 by the strain effect. *ACS applied materials & interfaces*, 6(16):14724–14728, 2014.

[53] Thaneshwor P Kaloni, YC Cheng, and Udo Schwingenschlögl. Electronic structure of superlattices of graphene and hexagonal boron nitride. *Journal of Materials Chemistry*, 22(3):919–922, 2012.

[54] Xiaoliang Zhong, Rodrigo G Amorim, Ralph H Scheicher, Ravindra Pandey, and Shashi P Karna. Electronic structure and quantum transport properties of trilayers formed from graphene and boron nitride. *Nanoscale*, 4(17):5490–5498, 2012.

[55] Shujie Tang, Guqiao Ding, Xiaoming Xie, Ji Chen, Chen Wang, Xuli Ding, Fuqiang Huang, Wei Lu, and Mianheng Jiang. Nucleation and growth of single crystal graphene on hexagonal boron nitride. *Carbon*, 50(1):329–331, 2012.

[56] Minhyeok Son, Hyunseob Lim, Misun Hong, and Hee Cheul Choi. Direct growth of graphene pad on exfoliated hexagonal boron nitride surface. *Nanoscale*, 3(8):3089–3093, 2011.

[57] Ashwin Ramasubramaniam, Doron Naveh, and Elias Towe. Tunable band gaps in bilayer graphene- bn heterostructures. *Nano letters*, 11(3):1070–1075, 2011.

[58] Yong-Jun Li, Qing-Qing Sun, Lin Chen, Peng Zhou, Peng-Fei Wang, Shi-Jin Ding, and David Wei Zhang. Hexagonal boron nitride intercalated multi-layer graphene: a possible ultimate solution to ultra-scaled interconnect technology. *AIP Advances*, 2(1):012191, 2012.

[59] D Stein, K v Klitzing, and G Weimann. Electron spin resonance on g a a s- al x ga 1- x as heterostructures. *Physical review letters*, 51(2):130, 1983.

[60] HL Stormer, Z Schlesinger, A Chang, DC Tsui, AC Gossard, and W Wiegmann. Energy structure and quantized hall effect of two-dimensional holes. *Physical review letters*, 51(2):126, 1983.

[61] Yu A Bychkov and Emmanuel I Rashba. Oscillatory effects and the magnetic susceptibility of carriers in inversion layers. *Journal of physics C: Solid state physics*, 17(33):6039, 1984.

[62] A Gamucci, D Spirito, M Carrega, B Karmakar, Antonio Lombardo, M Bruna, LN Pfeiffer, KW West, Andrea Carlo Ferrari, Marco Polini, et al. Anomalous low-temperature coulomb drag in graphene-gaas heterostructures. *Nature communications*, 5:5824, 2014.

[63] Shi-Sheng Lin, Zhi-Qian Wu, Xiao-Qiang Li, Yue-Jiao Zhang, Sheng-Jiao Zhang, Peng Wang, Rajapandiyan Panneerselvam, and Jian-Feng Li. Stable 16.2% efficient surface plasmon-enhanced graphene/gaas heterostructure solar cell. *Advanced Energy Materials*, 6(21):1600822, 2016.

[64] Yanghua Lu, Sirui Feng, Zhiqian Wu, Yixiao Gao, Jingliang Yang, Yuejiao Zhang, Zhenzhen Hao, Jianfeng Li, Erping Li, Hongsheng Chen, et al. Broadband surface plasmon resonance enhanced self-powered graphene/gaas photodetector with ultrahigh detectivity. *Nano Energy*, 47:140–149, 2018.

[65] Nguyen Van Men and Nguyen Quoc Khanh. Plasmon modes in graphene–gaas heterostructures. *Physics letters A*, 381(44):3779–3784, 2017.

[66] Nguyen Van Men and Dong Thi Kim Phuong. Plasmon modes in bilayer-graphene–gaas heterostructures including layer-thickness and exchange-correlation effects. *International Journal of Modern Physics B*, 32(23):1850256, 2018.

[67] Alexandre Tkatchenko and Matthias Scheffler. Accurate molecular van der waals interactions from ground-state electron density and free-atom reference data. *Physical review letters*, 102(7):073005, 2009.

[68] Pierre Hohenberg and Walter Kohn. Inhomogeneous electron gas. *Physical review*, 136(3B):B864, 1964.

[69] Walter Kohn and Lu Jeu Sham. Self-consistent equations including exchange and correlation effects. *Physical review*, 140(4A):A1133, 1965.

[70] Georg Kresse and Jürgen Furthmüller. Efficiency of ab-initio total energy calculations for metals and semiconductors using a plane-wave basis set. *Computational materials science*, 6(1):15–50, 1996.

[71] Georg Kresse and Jürgen Furthmüller. Efficient iterative schemes for ab initio total-energy calculations using a plane-wave basis set. *Physical review B*, 54(16):11169, 1996.

[72] John P Perdew, Kieron Burke, and Matthias Ernzerhof. Generalized gradient approximation made simple. *Physical review letters*, 77(18):3865, 1996.

[73] Peter E Blöchl. Projector augmented-wave method. *Physical review B*, 50(24):17953, 1994.

[74] Georg Kresse and D Joubert. From ultrasoft pseudopotentials to the projector augmented-wave method. *Physical Review B*, 59(3):1758, 1999.

[75] Hendrik J Monkhorst and James D Pack. Special points for brillouin-zone integrations. *Physical review B*, 13(12):5188, 1976.

[76] Atsushi Togo and Isao Tanaka. First principles phonon calculations in materials science.

*Scripta Materialia*, 108:1–5, 2015.

[77] AH Romero and F Munoz. Pyprocar code, 2015.

[78] Yvon Le Page and Paul Saxe. Symmetry-general least-squares extraction of elastic data for strained materials from ab initio calculations of stress. *Physical Review B*, 65(10):104104, 2002.

[79] OH Nielsen. Oh nielsen and rm martin, phys. rev. lett. 50, 697 (1983). *Phys. Rev. Lett.*, 50:697, 1983.

[80] Claude Cohen-Tannoudji, Bernard Diu, and Frank Laloe. Quantum mechanics, volume 2. *Quantum Mechanics, Volume 2, by Claude Cohen-Tannoudji, Bernard Diu, Frank Laloe, pp. 626. ISBN 0-471-16435-6. Wiley-VCH, June 1986.*, page 626, 1986.

[81] Luis EF Foa Torres, Stephan Roche, and Jean-Christophe Charlier. *Introduction to graphene-based nanomaterials: from electronic structure to quantum transport.* Cambridge University Press, 2014.

[82] Pekka Pyykko. Relativistic effects in structural chemistry. *Chemical Reviews*, 88(3):563–594, 1988.

[83] Xiaojun Wu, Yong Pei, and Xiao Cheng Zeng. B2c graphene, nanotubes, and nanoribbons. *Nano letters*, 9(4):1577–1582, 2009.

[84] K Kawahara, T Shirasawa, R Arafune, C-L Lin, T Takahashi, M Kawai, and N Takagi. Determination of atomic positions in silicene on ag (111) by low-energy electron diffraction. *Surface Science*, 623:25–28, 2014.

[85] Richard Charles Andrew, Refilwe Edwin Mapasha, Aniekan M Ukpong, and Nithaya Chetty. Mechanical properties of graphene and boronitrene. *Physical Review B*, 85(12):125428, 2012.

[86] Hemant Kumar, Dequan Er, Liang Dong, Junwen Li, and Vivek B Shenoy. Elastic deformations in 2d van der waals heterostructures and their impact on optoelectronic properties: predictions from a multiscale computational approach. *Scientific reports*, 5:10872, 2015.

[87] Sobhit Singh, Camilo Espejo, and Aldo H Romero. Structural, electronic, vibrational, and elastic properties of graphene/mos 2 bilayer heterostructures. *Physical Review B*, 98(15):155309, 2018.

[88] Debora Pierucci, Hugo Henck, Jose Avila, Adrian Balan, Carl H Naylor, Gilles Patriarche, Yannick J Dappe, Mathieu G Silly, Fausto Sirotti, AT Charlie Johnson, et al. Band alignment and minigaps in monolayer mos2-graphene van der waals heterostructures. *Nano letters*, 16(7):4054–4061, 2016.

[89] Graeme Henkelman, Andri Arnaldsson, and Hannes Jónsson. A fast and robust algorithm for bader decomposition of charge density. *Computational Materials Science*, 36(3):354–360, 2006.

[90] Sobhit Singh and Aldo H Romero. Giant tunable rashba spin splitting in a two-dimensional bisb monolayer and in bisb/aln heterostructures. *Physical Review B*, 95(16):165444, 2017.

[91] Weiyang Yu, Chun-Yao Niu, Zhili Zhu, Xiangfu Wang, and Wei-Bing Zhang. Atomically thin binary v–v compound semiconductor: a first-principles study. *Journal of Materials Chemistry C*, 4(27):6581–6587, 2016.

[92] Hui Zheng, Xian-Bin Li, Nian-Ke Chen, Sheng-Yi Xie, Wei Quan Tian, Yuanping Chen, Hong Xia, SB Zhang, and Hong-Bo Sun. Monolayer ii-vi semiconductors: A first-principles prediction. *Physical Review B*, 92(11):115307, 2015.

[93] B Sachs, TO Wehling, MI Katsnelson, and AI Lichtenstein. Adhesion and electronic structure of graphene on hexagonal boron nitride substrates. *Physical Review B*, 84(19):195414, 2011.

[94] Pablo San-Jose, A Gutiérrez-Rubio, Mauricio Sturla, and Francisco Guinea. Spontaneous strains and gap in graphene on boron nitride. *Physical Review B*, 90(7):075428, 2014.

[95] Qianku Hu, Qinghua Wu, Yanming Ma, Lijun Zhang, Zhongyuan Liu, Julong He, Hong Sun, Hui-Tian Wang, and Yongjun Tian. First-principles studies of structural and electronic properties of hexagonal b c 5. *Physical Review B*, 73(21):214116, 2006.

[96] Hongliang Shi, Hui Pan, Yong-Wei Zhang, and Boris I Yakobson. Quasiparticle band structures and optical properties of strained monolayer mos 2 and ws 2. *Physical Review B*, 87(15):155304, 2013.

[97] Gui Gui, Jin Li, and Jianxin Zhong. Band structure engineering of graphene by strain: first-principles calculations. *Physical Review B*, 78(7):075435, 2008.